Nonlinear chiral imaging of subwavelength-sized twisted-cross gold nanodimers

Mikko J. Huttunen,[1,*] Godofredo Bautista,[1] Manuel Decker,[2,3] Stefan Linden,[2,3,4] Martin Wegener,[2,3] and Martti Kauranen[1]

[1]*Department of Physics, Tampere University of Technology, FI-33101 Tampere, Finland*
[2]*Institut für Nanotechnologie, Karlsruhe Institute of Technology (KIT), Postfach 3640, D-76021 Karlsruhe, Germany*
[3]*Institut für Angewandte Physik and DFG-Center for Functional Nanostructures (CFN), Karlsruhe Institute of Technology (KIT), D-76128 Karlsruhe, Germany*
[4]*Physikalisches Institut, Universität Bonn, Nußallee 12, 53115 Bonn, Germany*
**mikko.j.huttunen@tut.fi*

Abstract: We perform second-harmonic generation (SHG) microscopy with circularly polarized (CP) light to measure chirality of individual twisted-cross gold nanodimers. The chiral signatures, based on different SHG response for the two CP components of incident light, are clearly visible even with off-resonance excitation. The SHG responses of individual nanodimers are found to vary by about a factor of five. The technique thus has very high sensitivity to the nanoscale deformations of the structure. The chiral signatures of the dimers, however, are found to be more uniform, and the technique is thus able to recognize the handedness of the twisted nanodimers with high reliability.

OCIS codes: (180.4315) Nonlinear microscopy; (190.4350) Nonlinear optics at surfaces; (160.1585) Chiral media; (160.3918) Metamaterials.

References and links

1. L. D. Barron, *Molecular Light Scattering and Optical Activity* (Cambridge University Press, 1982).
2. V. M. Shalaev, "Optical negative-index metamaterials," Nat. Photonics **1**(1), 41–48 (2007).
3. C. M. Soukoulis, S. Linden, and M. Wegener, "Negative refractive index at optical wavelengths," Science **315**(5808), 47–49 (2007).
4. A. S. Schwanecke, A. Krasavin, D. M. Bagnall, A. Potts, A. V. Zayats, and N. I. Zheludev, "Broken time reversal of light interaction with planar chiral nanostructures," Phys. Rev. Lett. **91**(24), 247404 (2003).
5. S. Tretyakov, I. Nefedov, A. Sihvola, S. Maslovski, and C. Simovski, "Waves and energy in chiral nihility," J. Electromagn. Waves Appl. **17**(5), 695–706 (2003).
6. J. B. Pendry, "A chiral route to negative refraction," Science **306**(5700), 1353–1355 (2004).
7. E. Plum, J. Zhou, J. Dong, V. A. Fedotov, T. Koschny, C. M. Soukoulis, and N. I. Zheludev, "Metamaterial with negative index due to chirality," Phys. Rev. B **79**(3), 035407 (2009).
8. S. Zhang, Y.-S. Park, J. Li, X. Lu, W. Zhang, and X. Zhang, "Negative refractive index in chiral metamaterials," Phys. Rev. Lett. **102**(2), 023901 (2009).
9. M. Kuwata-Gonokami, N. Saito, Y. Ino, M. Kauranen, K. Jefimovs, T. Vallius, J. Turunen, and Y. Svirko, "Giant optical activity in quasi-two-dimensional planar nanostructures," Phys. Rev. Lett. **95**(22), 227401 (2005).
10. M. Decker, M. W. Klein, M. Wegener, and S. Linden, "Circular dichroism of planar chiral magnetic metamaterials," Opt. Lett. **32**(7), 856–858 (2007).
11. A. V. Rogacheva, V. A. Fedotov, A. S. Schwanecke, and N. I. Zheludev, "Giant gyrotropy due to electromagnetic-field coupling in a bilayered chiral structure," Phys. Rev. Lett. **97**(17), 177401 (2006).
12. E. Plum, V. A. Fedotov, A. S. Schwanecke, N. I. Zheludev, and Y. Chen, "Giant optical gyrotropy due to electromagnetic coupling," Appl. Phys. Lett. **90**(22), 223113 (2007).
13. J. K. Gansel, M. Thiel, M. S. Rill, M. Decker, K. Bade, V. Saile, G. von Freymann, S. Linden, and M. Wegener, "Gold helix photonic metamaterial as broadband circular polarizer," Science **325**(5947), 1513–1515 (2009).
14. M. Thiel, M. S. Rill, G. von Freymann, and M. Wegener, "Three-dimensional bi-chiral photonic crystals," Adv. Mater. (Deerfield Beach Fla.) **21**(46), 4680–4682 (2009).
15. M. Decker, M. Ruther, C. E. Kriegler, J. Zhou, C. M. Soukoulis, S. Linden, and M. Wegener, "Strong optical activity from twisted-cross photonic metamaterials," Opt. Lett. **34**(16), 2501–2503 (2009).
16. M. Decker, R. Zhao, C. M. Soukoulis, S. Linden, and M. Wegener, "Twisted split-ring-resonator photonic metamaterial with huge optical activity," Opt. Lett. **35**(10), 1593–1595 (2010).

#142344 - $15.00 USD Received 7 Feb 2011; revised 4 Mar 2011; accepted 4 Mar 2011; published 22 Apr 2011

17. M. I. Stockman, D. J. Bergman, C. Anceau, S. Brasselet, and J. Zyss, "Enhanced second-harmonic generation by metal surfaces with nanoscale roughness: nanoscale dephasing, depolarization, and correlations," Phys. Rev. Lett. **92**(5), 057402 (2004).
18. M. W. Klein, C. Enkrich, M. Wegener, and S. Linden, "Second-harmonic generation from magnetic metamaterials," Science **313**(5786), 502–504 (2006).
19. M. W. Klein, M. Wegener, N. Feth, and S. Linden, "Experiments on second- and third-harmonic generation from magnetic metamaterials," Opt. Express **15**(8), 5238–5247 (2007).
20. N. Feth, S. Linden, M. W. Klein, M. Decker, F. B. P. Niesler, Y. Zeng, W. Hoyer, J. Liu, S. W. Koch, J. V. Moloney, and M. Wegener, "Second-harmonic generation from complementary split-ring resonators," Opt. Lett. **33**(17), 1975–1977 (2008).
21. F. B. P. Niesler, N. Feth, S. Linden, J. Niegemann, J. Gieseler, K. Busch, and M. Wegener, "Second-harmonic generation from split-ring resonators on a GaAs substrate," Opt. Lett. **34**(13), 1997–1999 (2009).
22. B. K. Canfield, H. Husu, J. Laukkanen, B. Bai, M. Kuittinen, J. Turunen, and M. Kauranen, "Local field asymmetry drives second-harmonic generation in non-centrosymmetric nanodimers," Nano Lett. **7**(5), 1251–1255 (2007).
23. H. Tuovinen, M. Kauranen, K. Jefimovs, P. Vahimaa, T. Vallius, J. Turunen, N. V. Tkachenko, and H. Lemmetyinen, "Linear and second-order nonlinear optical properties of arrays of noncentrosymmetric gold nanoparticles," J. Nonlinear Opt. Phys. Mater. **11**(4), 421–432 (2002).
24. B. K. Canfield, S. Kujala, K. Jefimovs, J. Turunen, and M. Kauranen, "Linear and nonlinear optical responses influenced by broken symmetry in an array of gold nanoparticles," Opt. Express **12**(22), 5418–5423 (2004).
25. B. K. Canfield, H. Husu, J. Kontio, J. Viheriala, T. Rytkonen, T. Niemi, E. Chandler, A. Hrin, J. A. Squier, and M. Kauranen, "Inhomogeneities in the nonlinear tensorial responses of arrays of gold nanodots," N. J. Phys. **10**(1), 013001 (2008).
26. B. K. Canfield, S. Kujala, K. Laiho, K. Jefimovs, J. Turunen, and M. Kauranen, "Chirality arising from small defects in gold nanoparticle arrays," Opt. Express **14**(2), 950–955 (2006).
27. S. Kujala, B. K. Canfield, M. Kauranen, Y. Svirko, and J. Turunen, "Multipole interference in the second-harmonic optical radiation from gold nanoparticles," Phys. Rev. Lett. **98**(16), 167403 (2007).
28. H. Husu, B. K. Canfield, J. Laukkanen, B. Bai, M. Kuittinen, J. Turunen, and M. Kauranen, "Chiral coupling in gold nanodimers," Appl. Phys. Lett. **93**(18), 183115 (2008).
29. P. M. Rentzepis, J. A. Giordmaine, and K. W. Wecht, "Coherent optical mixing in optically active liquids," Phys. Rev. Lett. **16**(18), 792–794 (1966).
30. A. P. Shkurinov, A. V. Dubrovskii, and N. I. Koroteev, "Second harmonic generation in an optically active liquid: Experimental observation of a fourth-order optical nonlinearity due to molecular chirality," Phys. Rev. Lett. **70**(8), 1085–1088 (1993).
31. P. Fischer, D. S. Wiersma, R. Righini, B. Champagne, and A. D. Buckingham, "Three-wave mixing in chiral liquids," Phys. Rev. Lett. **85**(20), 4253–4256 (2000).
32. M. A. Belkin, T. A. Kulakov, K.-H. Ernst, L. Yan, and Y. R. Shen, "Sum-frequency vibrational spectroscopy on chiral liquids: a novel technique to probe molecular chirality," Phys. Rev. Lett. **85**(21), 4474–4477 (2000).
33. M. Kauranen, T. Verbiest, and A. Persoons, "Second-order nonlinear optical signatures of surface chirality," J. Mod. Opt. **45**(2), 403–423 (1998).
34. J. Hicks, *Chirality: Physical Chemistry*, *ACS Symposium Series 810* (American Chemical Society, 2002).
35. S. Sioncke, T. Verbiest, and A. Persoons, "Second-order nonlinear optical properties of chiral materials," Mater. Sci. Eng. Rep. **42**(5-6), 115–155 (2003).
36. M. A. Belkin and Y. R. Shen, "Non-linear optical spectroscopy as a novel probe for molecular chirality," Int. Rev. Phys. Chem. **24**(2), 257–299 (2005).
37. T. Verbiest, M. Kauranen, Y. Van Rompaey, and A. Persoons, "Optical activity of anisotropic achiral surfaces," Phys. Rev. Lett. **77**(8), 1456–1459 (1996).
38. M. Siltanen, E. Vuorimaa, H. Lemmetyinen, P. Ihalainen, J. Peltonen, and M. Kauranen, "Nonlinear optical and structural properties of langmuir-blodgett films of thiohelicenebisquinones," J. Phys. Chem. B **112**(7), 1940–1945 (2008).
39. V. A. Makarov and I. A. Perezhogin, "Generation of reflected second-harmonic light beam with inhomogeneous transversal distribution of polarization from the surface of chiral medium by normally incident Gaussian beam," Opt. Commun. **281**(14), 3906–3912 (2008).
40. M. J. Huttunen, M. Erkintalo, and M. Kauranen, "Absolute nonlinear optical probes of surface chirality," J. Opt. A, Pure Appl. Opt. **11**(3), 034006 (2009).
41. M. J. Huttunen, M. Virkki, M. Erkintalo, E. Vuorimaa, A. Efimov, H. Lemmetyinen, and M. Kauranen, "Absolute probe of surface chirality based on focused circularly polarized light," J. Phys. Chem. Lett. **1**(12), 1826–1829 (2010).
42. T. Petralli-Mallow, T. M. Wong, J. D. Byers, H. I. Yee, and J. M. Hicks, "Circular dichroism spectroscopy at interfaces: A surface second harmonic generation study," J. Phys. Chem. **97**(7), 1383–1388 (1993).
43. J. D. Byers, H. I. Yee, and J. M. Hicks, "A second harmonic generation analog of optical rotator dispersion for the study of chiral monolayers," J. Chem. Phys. **101**(7), 6233–6241 (1994).
44. J. D. Byers, H. I. Yee, T. Petralli-Mallow, and J. M. Hicks, "Second-harmonic generation circular-dichroism spectroscopy from chiral monolayers," Phys. Rev. B Condens. Matter **49**(20), 14643–14647 (1994).

#142344 - $15.00 USD Received 7 Feb 2011; revised 4 Mar 2011; accepted 4 Mar 2011; published 22 Apr 2011

45. M. Kauranen, T. Verbiest, J. J. Maki, and A. Persoons, "Second-harmonic generation from chiral surfaces," J. Chem. Phys. **101**(9), 8193–8199 (1994).
46. T. Verbiest, M. Kauranen, J. J. Maki, M. N. Teerenstra, A. J. Schouten, R. J. M. Nolte, and A. Persoons, "Linearly polarized probes of surface chirality," J. Chem. Phys. **103**(18), 8296–8298 (1995).
47. J. J. Maki, T. Verbiest, M. Kauranen, S. V. Elshocht, and A. Persoons, "Comparison of linearly and circularly polarized probes of second-order optical activity of chiral surfaces," J. Chem. Phys. **105**(2), 767–772 (1996).
48. M. C. Schanne-Klein, F. Hache, A. Roy, C. Flytzanis, and C. Payrastre, "Off resonance second order optical activity of isotropic layers of chiral molecules: Observation of electric and magnetic contributions," J. Chem. Phys. **108**(22), 9436–9443 (1998).
49. G. J. Simpson, "Molecular origins of the remarkable chiral sensitivity of second-order nonlinear optics," ChemPhysChem **5**(9), 1301–1310 (2004).
50. S. A. Mitchell and R. A. McAloney, "Second harmonic optical activity of tryptophan derivatives adsorbed at the air/water interface," J. Phys. Chem. B **108**(3), 1020–1029 (2004).
51. M. A. Kriech and J. C. Conboy, "Counterpropagating second-harmonic generation: A new technique for the investigation of molecular chirality at surfaces," J. Opt. Soc. Am. B **21**(5), 1013–1022 (2004).
52. M. A. Kriech and J. C. Conboy, "Imaging chirality with surface second harmonic generation microscopy," J. Am. Chem. Soc. **127**(9), 2834–2835 (2005).
53. N. Ji, K. Zhang, H. Yang, and Y. R. Shen, "Three-dimensional chiral imaging by sum-frequency generation," J. Am. Chem. Soc. **128**(11), 3482–3483 (2006).
54. G. Subramania and S. Y. Lin, "Fabrication of three-dimensional photonic crystal with alignment based on electron beam lithography," Appl. Phys. Lett. **85**(21), 5037–5039 (2004).
55. N. Liu, H. Liu, S. Zhu, and H. Giessen, "Stereometamaterials," Nat. Photonics **3**(3), 157–162 (2009).
56. V. K. Valev, N. Smisdom, A. V. Silhanek, B. De Clercq, W. Gillijns, M. Ameloot, V. V. Moshchalkov, and T. Verbiest, "Plasmonic ratchet wheels: switching circular dichroism by arranging chiral nanostructures," Nano Lett. **9**(11), 3945–3948 (2009).
57. V. K. Valev, A. V. Silhanek, N. Smisdom, B. De Clercq, W. Gillijns, O. A. Aktsipetrov, M. Ameloot, V. V. Moshchalkov, and T. Verbiest, "Linearly polarized second harmonic generation microscopy reveals chirality," Opt. Express **18**(8), 8286–8293 (2010).
58. V. K. Valev, A. V. Silhanek, N. Verellen, W. Gillijns, P. Van Dorpe, O. A. Aktsipetrov, G. A. Vandenbosch, V. V. Moshchalkov, and T. Verbiest, "Asymmetric optical second-harmonic generation from chiral G-shaped gold nanostructures," Phys. Rev. Lett. **104**(12), 127401 (2010).

1. Introduction

Chirality is a fundamental symmetry property of materials, referring to lack of reflection/inversion symmetry in the material system [1]. Chiral molecules thus occur in two mirror-image forms (enantiomers), which cannot be superimposed on top of each other. Chiral materials interact differently with the two circularly polarized (CP) components of light, which give rise to optical activity (OA) effects, such as polarization rotation and circular dichroism [1]. The circular-difference (CD) effects reverse sign between the two enantiomers of a chiral molecule. For isotropic solutions of chiral molecules, the OA effects arise from lowest-order magnetic contributions to the optical response [1]. Due to its relation to broken inversion symmetry, chirality is inherently associated with three-dimensional (3D) molecular structures.

The development of advanced nanofabrication techniques has led to the new research field of metamaterials [2,3], where chirality is an important issue [4]. Chirality has been proposed as an interesting way to achieve negative index of refraction [5–8]. In addition, precise engineering of the structural properties of chiral metamaterials can lead to artificial sub-wavelength features that give rise to giant and broadband OA effects [9–16], which open intriguing possibilities in nanoscale polarization control. Such materials often consist of two-dimensional (2D) arrays of metal nanoparticles. Nevertheless, even then chiral effects arise from the 3D character of real samples [9,10]. In fact, strong polarization effects have been observed with structures that have been designed to be 3D, including double-layer structures, where the interaction in the vertical direction plays a key role [11–16].

Metal nanoparticles are interesting also for nonlinear optics. This is because their plasmonic and magnetic resonances support strong local fields, which can drive the nonlinear responses efficiently [17]. Second-harmonic generation (SHG), e.g., has been observed from split-ring resonators [18–21], T-shaped nanodimers [22], and L-shaped nanoparticles [23,24]. Second-order effects, however, are extremely sensitive to the structural symmetry of the

#142344 - $15.00 USD Received 7 Feb 2011; revised 4 Mar 2011; accepted 4 Mar 2011; published 22 Apr 2011

samples, with chirality and anisotropy having their unique signatures in the polarization-dependent nonlinear responses [23–25]. In fact, this sensitivity is so high that even effects arising from undesired symmetry breaking, including shape distortions and surface defects, affect the responses [26–28]. For metal nanostructures, the overall second-order response thus arises from a complicated interplay between the plasmonic resonances of the particles and their structural defects. This is in strong contrast with the linear optical responses, which can be well predicted by the overall features of the particles.

Another interesting aspect is that, by definition, chirality breaks the centrosymmetry of materials. Chiral materials therefore always have a nonvanishing second-order nonlinear optical response. This occurs even when the material is otherwise highly symmetric, including isotropic materials [29–32]. From the point of view of metamaterials research, chiral nanostructures could thus lead to an intriguing new class of nonlinear materials.

Chiral nanostructures and nonlinear optics thus have two complementary connections. First, nonlinear techniques can provide new probes of chirality to investigate the properties of nanostructures beyond what is possible by linear optical techniques. Second, chiral nanostructures could lead to new types of second-order materials with optimized nonlinear responses. For both aspects, it is essential to develop the basic understanding as to what types of nonlinear schemes couple significantly with the chiral properties of nanostructured materials in the presence of possible imperfections of state-of-the-art samples.

SHG has earlier been used to probe chiral properties of molecular films [33–36]. In the standard geometry of surface SHG, chirality leads to a different SHG response for the two CP components of fundamental light. Unfortunately, such techniques are compromised by possible in-plane anisotropy of the thin-film sample, which can also lead to such a second-harmonic generation circular-difference (SHG-CD) response [37]. This problem arises because the orientation of the anisotropic sample can make the experimental setup chiral. Separation of chirality and anisotropy is thus a significant problem [38] and a particular concern for metamaterials, where the unintended structural features may lead to anisotropy of chiral samples and vice versa. The separation problem can be overcome by increasing the symmetry of the experimental geometry. More specifically, SHG microscopy with a focused CP fundamental beam at normal incidence is only sensitive to chirality, but not to anisotropy [39–41].

In this paper, we demonstrate that SHG microscopy can be used to probe chirality of individual nano-objects, which consist of double-layer twisted-cross gold nanodimers [15]. In order to avoid the false chiral signatures, our technique is based on measuring the different SHG response of the objects for both handedness of CP fundamental light at normal incidence. We find that the SHG responses of individual twisted nanodimers vary. Nevertheless, a twisted-cross of a given handedness has strong preference for one CP and this preference is opposite for the two enantiomers. On the other hand, the normalized SHG-CD response is more uniform. Our results show that SHG microscopy provides a sensitive tool to investigate both the chiral properties of metamaterials and the quality of the samples.

2. Chiral probes based on second-harmonic generation

SHG has been found to be extremely sensitive and highly versatile probe to investigate the chirality of molecules, solutions and thin films [33–36,38–52], and more recently also in the study of metal nanostructures [18–28]. The sensitivity of SHG to chirality originates from its intrinsic sensitivity to symmetry properties. Another advantage of such nonlinear chiral probes is that, unlike linear OA effects, they are allowed within the electric-dipole approximation of the light-matter interaction. Because of this argument, the relative strength of SHG-CD can be on the order of unity and orders of magnitude greater than the relative strength of linear effects, which are typically on the order of $\Delta n / n \sim 10^{-3}$ or less for the index of refraction for the two circular polarizations [43].

#142344 - $15.00 USD Received 7 Feb 2011; revised 4 Mar 2011; accepted 4 Mar 2011; published 22 Apr 2011

SHG-based chiral probes usually rely on different efficiency of SHG for the two CP components of fundamental light. In addition to CP light, and the corresponding SHG-CD response, linearly-polarized light and the corresponding SHG linear-difference (SHG-LD) response have been shown to be chirality-sensitive [43,46]. For molecular thin films, the second-order susceptibility tensor components involving the surface normal are usually important. Typical experiments with collimated beams are therefore performed at oblique incidence [42–50] to generate polarization components along the normal.

The traditional techniques work well under the assumption that the sample has in-plane isotropy, i.e., full rotational symmetry about the surface normal. However, if the sample has in-plane anisotropy, these techniques are compromised because the orientation of the anisotropy axis can make the experiment chiral, which can also give rise to a SHG-CD response [37]. Discrimination between anisotropy and chirality can be achieved by a technique, which involves azimuthal rotation of the sample about its surface normal [38]. It is evident that this approach is not suitable for nonlinear microscopy. On the other hand, we have recently developed a simple SHG technique, which is capable of distinguishing chirality from anisotropy in an unambiguous manner [40,41]. The technique is based on strong focusing of CP light at normal incidence, making the experimental setup rotationally symmetric and thus insensitive to anisotropy. The technique is thus naturally applicable to SHG microscopy of chiral properties even for anisotropic samples, which is not the case in earlier second-order techniques for chiral microscopy, which have implicitly assumed that the sample has in-plane isotropy [51–53].

For molecular films, the technique can be understood on the basis of the nonvanishing components of the second-order susceptibility tensor for various chiral and/or anisotropic symmetry groups and their coupling to all three field components in the focal volume [39,40]. The SHG-CD response can then be shown to arise from interference between the achiral and chiral tensor components [33,43–45], where the latter change sign between the two enantiomers. The susceptibility tensor thus determines the SHG signals that can be measured and their relative strengths.

In the present work, however, we study metal nanodimers, which are known to modify the local-field distribution in the structure. Furthermore, the vectorial local field can contain components not present in the beam incident on the particles [22]. At this time, it is not feasible to track the local fields and their interaction with the local susceptibility tensors. This is not a problem in our measurement technique, however, because the possible SHG signals and their strengths are still determined by the overall symmetry of the nanodimers. In particular, we still expect different SHG response for the two CP components of fundamental light when the sample is chiral, independent of whether it has in-plane anisotropy or not.

The SHG-CD response is best described by the normalized quantity [47]

$$\text{SHG-CD} = \frac{\Delta P_{\text{SHG-CD}}}{P_{\text{AVE}}} = \frac{P_{\text{LHCP}} - P_{\text{RHCP}}}{(P_{\text{LHCP}} + P_{\text{RHCP}})/2}, \tag{1}$$

where P is the collected SHG power and the subscripts LHCP and RHCP indicate the left-hand and right-hand CP components of the fundamental beam. Note that this quantity is defined in such a way that it varies between –2 and 2.

3. Second-harmonic generation microscopy

To characterize the nonlinear response and chirality of the sample, we used a custom-built SHG microscope with CP light as depicted in Fig. 1. A mode-locked Nd:glass laser (Time Bandwidth, Switzerland; fundamental wavelength 1060 nm; pulse width 200 fs; repetition rate 82 MHz; maximum average output power 300 mW) is used as a source of fundamental light. A pinhole-expander assembly (PH, L1, L2) is then used to spatially filter and expand the laser beam. The resulting collimated beam with a diameter of 7 mm is directed to the back-aperture

#142344 - $15.00 USD Received 7 Feb 2011; revised 4 Mar 2011; accepted 4 Mar 2011; published 22 Apr 2011

of an infinity-corrected microscope objective (O1; Nikon LU PLAN Fluor 50 × /NA = 0.80), which then focuses the beam on the sample. This objective is strain-free and was chosen to minimize any undesired polarization deformations when focusing. The focal spot has a waist diameter of 800 nm.

The linear polarization of the fundamental beam is first cleaned up with a calcite polarizer (P) and then controlled with a motorized quarter-wave plate (QWP; Newport) to access the CP states. In particular, the QWP rotation angles of 0°/180° and 90°/270° correspond to right-hand CP (RHCP) and left-hand CP (LHCP) beams.

The transmitted SHG signals were collected by a second microscope objective (O2; Olympus PLAN N 20 × /NA = 0.40). We emphasize that no analyzer was used after O2 to avoid any false chiral effects from the measurement geometry. We used a fundamental wavelength-blocking filter (FF), a narrowband interference filter (IF; 530 nm) and a tube lens (L3) to discriminate and focus the SHG signal onto a cooled photomultiplier tube (PMT).

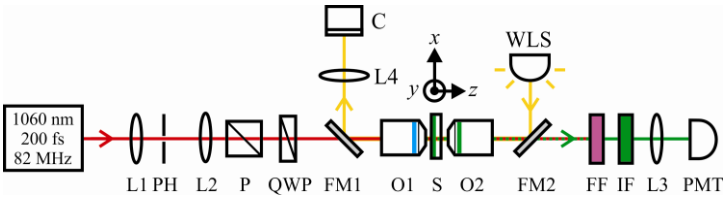

Fig. 1. Schematic diagram of the SHG microscope used for characterizing the nonlinear response and chirality of the twisted-cross nanodimers. The optical setup consists of lenses (L1,L2,L3,L4), pinhole (PH), polarizer (P), motorized quarter-wave plate (QWP), microscope objectives (O1,O2), 3-axis motorized stage (S), flip mirrors (FM1,FM2), fundamental wavelength-blocking filter (FF), interference filter (IF), photomultiplier tube (PMT), white light source (WLS) and camera (C). Ray path colors: fundamental excitation wavelength (red), frequency doubled SHG signal (green), white light (yellow).

The sample is mounted on a 3-axis motorized translation stage (S; Thorlabs MAX301/M) to allow sample scanning. In order to acquire SHG images as a function of sample location, the sample was scanned in the transverse directions across the focal spot in steps of 50 nm. The pixel acquisition time was 5 ms and every single pixel measurement was repeated 4 times and averaged to form the actual pixel value. Note that sample (instead of beam) scanning is preferable to maintain the polarization purity of the fundamental beam in the focal volume. The scanning was accomplished by using a custom program written in LabVIEW. The microscope also included a secondary imaging arm, which consists of a white light source (WLS), two flip mirrors (FM1, FM2), tube lens (L4) and camera (C) to view a specific area of the sample before nonlinear imaging.

4. Double-layer twisted-cross chiral gold nanodimers

Our samples consist of a double-layer structure where each layer itself consists of an array of achiral gold crosses [15]. The chirality arises from the mutual orientation of the crosses in the two layers (Fig. 2) and is therefore directly associated with the 3D character of the structure. A relative twist angle of 22.5° between the crosses in the two layers was chosen to make the unit cell of the double-layer array chiral. The samples were fabricated using a layer-by-layer approach involving electron-beam lithography and spin-on glass planarization [54,55]. Electron-beam lithography was used for the first layer of crosses, which were prepared on a glass substrate covered with a 5 nm thin film of indium-tin-oxide (ITO). In the next step, the surface was planarized with commercial spin-on dielectric (IC1-200, Futurex, Inc.). The dielectric layer was then made thinner by reactive ion etching (SF 6, Plasmalab80Plus, Oxford Instruments Plasma Technology). Finally, a second layer of crosses was fabricated using electron-beam lithography. Great care was taken to align the crosses in the second layer on top of those in the first layer, and maximum misalignment was smaller than 10 nm over the entire sample area. The resulting fabricated crosses are 25 nm thick and separated by a 35 nm

#142344 - $15.00 USD Received 7 Feb 2011; revised 4 Mar 2011; accepted 4 Mar 2011; published 22 Apr 2011

thick spacer. For the present work, where the goal is to address individual chiral nano-objects, the relevant entity is thus a twisted-cross nanodimer, which consists of the two achiral crosses on top of each other. Ideally, the nanodimers belong to the point group symmetry C_4, which for the linear and second-order responses is equivalent to in-plane isotropy.

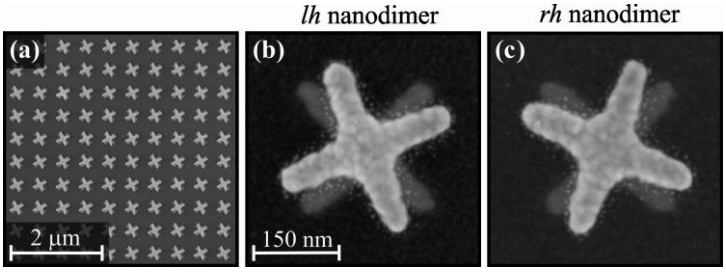

Fig. 2. Large-area electron micrograph of the fabricated twisted-cross nanodimers (a). Close-up views of the *lh* (b) and *rh* (c) twisted-cross nanodimers consisting of two achiral crosses on top of each other.

The twisted-cross nanodimers were ordered in a square array with a 500 nm period. These dimers covered an area of 100 μm x 100 μm. We emphasize that good overall sample quality was achieved as can be clearly seen from Fig. 2(a). Both left-handed (*lh*) and right-handed (*rh*) twisted-cross nanodimers [Figs. 2(b) and 2(c)] were fabricated on the same substrate.

The samples have earlier been characterized by linear transmittance spectroscopy and have been shown to exhibit two distinct resonances, which correspond to the effective oscillation modes of the two coupled crosses [15]. The two resonances occur at wavelengths of 1200 nm and 1550 nm, which are somewhat longer than the fundamental wavelength used in the SHG measurements. The samples have also been reported to exhibit pronounced circular dichroism at the resonance wavelengths and displayed significant optical activity between the two resonances. The linear optical properties are well described by the common approaches for electromagnetic modeling. In the present paper, however, we utilize SHG microscopy to investigate the nonlinear response of the twisted-cross dimers. This technique is expected to be sensitive to the overall chiral structure of the dimers. However, the response may also be modified by the nanoscale surface roughness evident in Figs. 2(a) and 2(b) as well as *in situ* laser-induced damage.

The samples were characterized microscopically by using an average laser power of 5 mW before the illuminating objective (O1) in our microscope (Fig. 1). This power setting provided reasonably detectable SHG signals from the dimers and was significantly smaller than the threshold power estimate of 20 mW from which photodamage at the focal region is observed. At this chosen power level, we obtained highly repeatable microscopy images of the dimers. It is also worth noting that the detected nonlinear responses from the nanodimers actually emanated from the focal region. This was evidenced by rapid attenuation of the measured SHG signals when the sample was moved in small axial displacements away from the focal region.

5. Results and discussions

Representative images acquired using the transmitted SHG signals are shown in Fig. 3 for the *lh* and *rh* twisted-cross samples excited by the LHCP and RHCP fundamental light. The first general observation is that the SHG signals exhibit variations with the 500-nm periodicity of the array. Even though this periodicity is sub-wavelength for the fundamental laser used, our microscope is able to address the overall response of the individual dimers. Another important observation is that the SHG responses of the individual dimers vary, which is better seen from Y-stacked composite SHG line profiles [Figs. 3(c), 3(d), 3(g) and 3(h)]. The peak-to-peak variation of the SHG intensity is about a factor of five. We believe that the strongest

#142344 - $15.00 USD Received 7 Feb 2011; revised 4 Mar 2011; accepted 4 Mar 2011; published 22 Apr 2011

individual hot spots in the images are due to localized defects in some of the dimers, which support particularly strong local fields at the wavelength of our laser and for the particular polarization used. On the other hand, the RMS variation in the SHG signals is on the order of 30%. The detected SHG intensity scales with the square of the effective nonlinear susceptibility of each dimer, which is the fundamental quantity associated with the structure. We may therefore argue that, on the average and in terms of their SHG response, the individual dimers differ from the average by about 15%.

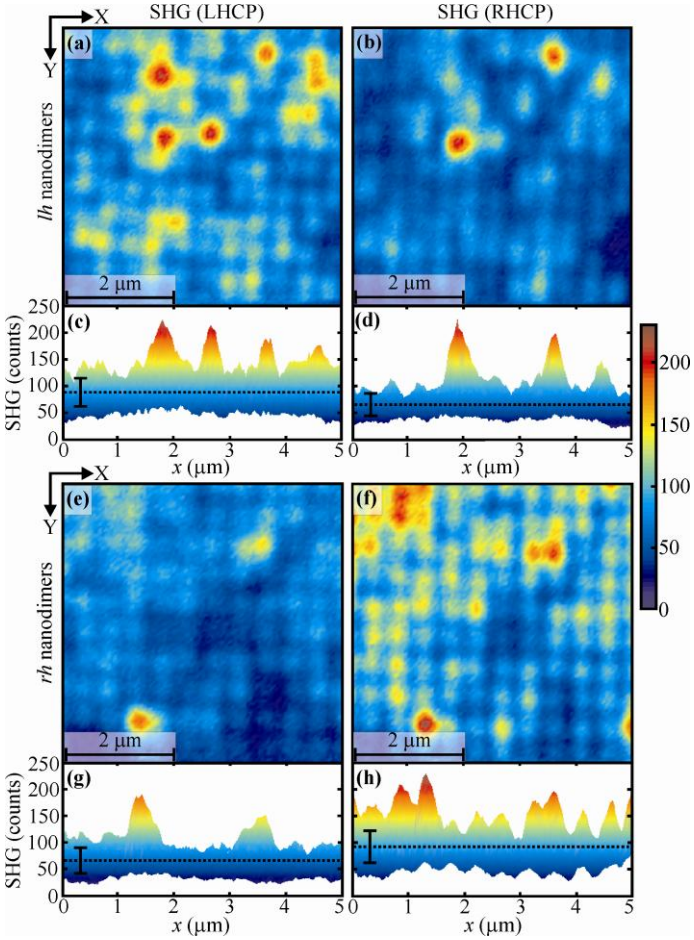

Fig. 3. SHG images of *lh* and *rh* twisted-cross nanodimers using LHCP [(a) and (e)] and RHCP [(b) and (f)] fundamental beam. Y-stacked composite SHG line profiles of the *lh* [(c) and (d)] and *rh* [(g) and (h)] nanodimers illustrate the signal variation. Average SHG values are shown as black dotted lines [(c), (d), (g) and (h)] together with the calculated standard deviation bars.

In spite of the local variations in the SHG responses of the individual dimers, our technique has very good sensitivity to the chirality of the dimers. The *lh* twisted dimers clearly give a stronger SHG signal for the LHCP fundamental light [Figs. 3(a) to 3(d)], whereas the *rh* dimers prefer the RHCP light [Figs. 3(e) to 3(h)]. Interestingly, such chiral signatures, based on different SHG response for the two CP components of incident light, are clearly visible even with off-resonance excitation.

In order to analyze this further, we present the normalized SHG-CD images and Y-stacked composite line profiles of the two samples in Fig. 4. The local CD responses are seen to be more uniform than the original SHG signals, which is evident especially by comparing the Y-stacked composite SHG line profiles [Figs. 3(c), 3(d), 3(g) and 3(h)] and SHG-CD [Figs. 4(c)

#142344 - $15.00 USD Received 7 Feb 2011; revised 4 Mar 2011; accepted 4 Mar 2011; published 22 Apr 2011

and 4(d)]. More importantly, the average SHG signals of Fig. 3 for the two polarizations are within each other's error bars, whereas those of the SHG-CD response of Fig. 4 are not. The SHG-CD responses averaged over the whole image area are found to be –0.32 for the *lh* and 0.35 for the *rh* structures. The almost equal magnitudes and opposite signs are in excellent agreement with the expected result. Regardless of the few individual dimers that give rise to a SHG-CD response of the wrong sign, the CD response is thus strongly correlated with the handedness of the dimer.

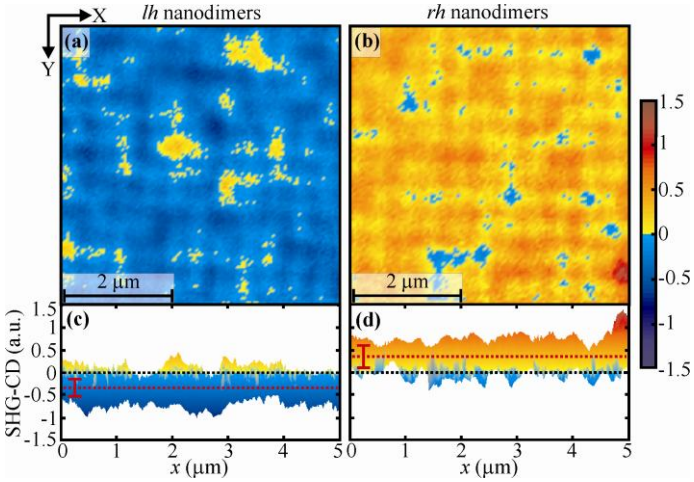

Fig. 4. SHG-CD images of *lh* (a) and *rh* (b) twisted-cross nanodimers derived using the images in Fig. 3. Y-stacked composite SHG-CD line profiles [(c) and (d)] illustrate the pixelwise SHG-CD values of (a) and (b). Coloring highlights the sign of the response and thus the chirality of the structures. Averaged SHG-CD responses of the scanned areas are –0.32 and 0.35 for the *lh* and *rh* structures, respectively. Those are shown as red dotted lines in (c) and (d) together with the calculated standard deviation bars. Zero reference levels are marked as black dotted lines in (c) and (d).

To estimate the reliability of the SHG-CD response in detecting the handedness of the individual dimers, we calculated the percentages of pixels with the proper sign of the CD response for the *lh* and *rh* twisted dimers, which were 93% and 95%, respectively. In addition, the CD responses with the wrong sign do not arise from the limitations of the technique but are related to the properties of the sample. Furthermore, the SHG-CD responses of the wrong sign are at least partly related to the presence of exceptionally strong SHG signals, e.g., the two very bright dimers in Fig. 3(b). As already mentioned, such very bright signals are most likely due to strongly favorable defects of the particular dimer for efficient SHG. These results imply that we are able to recognize the handedness of individual nanodimers quite reliably even though their overall SHG responses vary.

We next return to the possible role of defects in SHG from the present samples. Our twisted dimers belong ideally to the point group symmetry C_4, which is equivalent to in-plane isotropy of the sample for SHG. For this symmetry, SHG signals can only be generated in the presence of field components in the direction of the sample normal [39–41]. Our microscopic technique gives rise to such longitudinal field components even when the experiment is performed at normal incidence. Under our focusing conditions, however, the field amplitudes of the longitudinal components remain an order of magnitude weaker than the transverse components.

Any defects of an individual dimer, however, can break its ideal symmetry and give rise to in-plane anisotropy and in-plane chirality. This would allow SHG even with in-plane field components. If such symmetry breaking effects were strong, we would expect both the SHG signals and the SHG-CD responses to vary essentially randomly from one dimer to another.

#142344 - $15.00 USD Received 7 Feb 2011; revised 4 Mar 2011; accepted 4 Mar 2011; published 22 Apr 2011

This is particularly so because the transverse field components are significantly stronger than the longitudinal components. For the present samples, however, the SHG signals vary more than the SHG-CD responses. This suggests that the role of the defects is to influence mainly the coupling of the dimers to the longitudinal field components, but not to break the in-plane symmetry of the samples. Such effects would thus mainly affect the absolute SHG signals but be less important for the SHG-CD response. The results of the SHG measurements thus suggest that the overall quality of the samples is very good.

We finally note that other authors have also used SHG to address chiral nanostructures in a traditional surface SHG setup [56–58]. Their samples consisted of single-layer arrays of G-shaped metal structures. Both SHG-CD [56] and SHG-LD [57,58] effects were observed. The SHG-CD response was shown to arise from supraelement level in which the relative orientation of the adjacent particles was crucial, although even individual G's are chiral. Furthermore, the size of the G particles was about 1 μm wide. The particles were thus larger than the 800 nm wavelength of the laser used. Consequently, in the microscopic measurements, the authors were able to address parts of individual particles and attempted to correlate them to the possible hot spots of the local-field distribution. In contrast to this, our twisted-cross nanodimers have sub-wavelength size. We have therefore measured the overall response of the individual dimers, which is more directly associated with its structural symmetry independent of the details of the local-field distribution within the dimers.

6. Conclusion

In conclusion, we have demonstrated that second-harmonic generation microscopy with circularly polarized light can be utilized to probe chirality of individual subwavelength-sized objects. The technique is very sensitive to nanoscale structural features of metal nanoparticles, where the overall second-harmonic response arises from a complicated interplay of the plasmonic resonances of individual particles and their structural defects. For samples of low quality, the response could even be dominated by symmetry-breaking defects of the structure.

In the present paper, the technique was applied to double-layer twisted-cross chiral gold nanodimers organized in a two-dimensional array. Our microscope was able to resolve individual dimers, whose second-harmonic responses were found to vary significantly. Although the RMS variation in the responses was relatively small, some nanodimers were found to lead to significantly higher second-harmonic response. This behavior was explained by the nanoscale defects of the particular dimers that are favorable for efficient second-harmonic generation for the wavelength and circular polarization used.

In spite of the large variations in the second-harmonic responses of individual dimers, the general observation is that dimers of a given handedness lead to stronger second-harmonic generation for one circular polarization of fundamental light than the other. For the samples investigated, the average circular-difference response in the second-harmonic efficiency was on the order of 0.35. The circular-difference response was also found to vary between individual nanodimers. Importantly, however, the circular-difference response was significantly more uniform than the second-harmonic signals themselves. The technique thus provides a reliable way to address the handedness of chiral nano-objects.

Due to its superior sensitivity to the structural features of nano-objects and their chiral properties, we expect polarized second-harmonic generation microscopy to become a useful tool in the characterization of the quality and symmetry of nanostructures. In the future, it will also be interesting to extend the technique from circular-difference effects to a more complete tensor analysis of the nonlinear response of individual nanoparticles.

Acknowledgements

This work was funded by the ANIMOS Consortium project under the Research Program on Photonics and Modern Imaging Techniques of the Academy of Finland (project 134973). MJH acknowledges support from the Graduate School of Modern Optics and Photonics in

Finland. The Karlsruhe team acknowledges support by the Deutsche Forschungsgemeinschaft (DFG), the State of Baden-Württemberg, and the Karlsruhe Institute of Technology (KIT) through the DFG Center for Functional Nanostructures (CFN) within subproject A1.5. The project PHOME acknowledges the financial support of the Future and Emerging Technologies (FET) programme within the Seventh Framework Programme for Research of the European Commission, under FET-Open grant number 213390. The project METAMAT is supported by the Bundesministerium für Bildung und Forschung (BMBF).

#142344 - $15.00 USD Received 7 Feb 2011; revised 4 Mar 2011; accepted 4 Mar 2011; published 22 Apr 2011